

# Software framework and method for the alignment of the LHCb RICH optical system using proton-proton collisions during LHC Run II

XXX<sup>1</sup>.

<sup>1</sup>*University of Bristol, Bristol, United Kingdom*

## Abstract

The method for aligning the optical system of the LHCb Ring-Imaging Cherenkov (RICH) detectors during Run II of the Large Hadron Collider (LHC) is presented. The alignment will run online, within the high performance trigger system, and will be performed for each LHC fill. The alignment method for the RICH detectors is outlined, as well as its implementation in a novel online framework. The performance and stability of the alignments over the 2015 data taking period is shown.



# 1 Introduction

The LHCb experiment uses two ring-imaging Cherenkov (RICH) detectors to provide powerful discrimination between charged particles in the intense hadron production environment of the LHC. These two separate RICH detectors have different radiators and are designed to provide particle identification over a momentum range of 1 to 100 GeV/c [1]. The performance of the particle identification supplied by the RICH system [2] strongly depends on the quality of its alignment, i.e. how accurately the physical position of each component of the RICH detectors is described in the LHCb software. The goal of the alignment procedure is determine the exact position of all optical components and propagate this information to the LHCb conditions database that stores the non-event time-varying data pertaining to detector conditions. The LHCb detector achieved excellent performance in Run I but faces more challenging conditions in Run II. The LHC will collide protons at an increased centre-of-mass energy of 13 TeV and with 25 ns bunch spacing. The spatial alignment of the detector and the accurate calibration of its subcomponents are essential to achieve the best physics performance. In order to keep the selection efficiencies in the high level trigger as high as in Run I, conditions on the particle identification will be used in Run II. This requires the full alignment and calibration of the RICH detectors within the high performance trigger sequence. This note describes how the LHCb RICH optical systems are aligned in software in Run II using proton-proton collision data. The method used is discussed in Sec. 3, while the computing framework and the implementation for the automated running of the alignment is described in Sec. 4. The results for the data-taking period in 2015 are presented in Section ??.

$$O = \frac{\sum^{ADC > thresh.} N_{events}}{\sum N_{events}} \quad (1)$$

## 2 The LHCb detector

The LHCb detector [1, 3] is a single-arm forward spectrometer covering the pseudorapidity range  $2 < \eta < 5$ , designed for the study of particles containing  $b$  or  $c$  quarks. The detector includes a high-precision tracking system consisting of a silicon-strip vertex detector surrounding the  $pp$  interaction region, a large-area silicon-strip detector located upstream of a dipole magnet with a bending power of about 4 Tm, and three stations of silicon-strip detectors and straw drift tubes placed downstream of the magnet. The tracking system provides a measurement of momentum,  $p$ , of charged particles with a relative uncertainty that varies from 0.5% at low momentum to 1.0% at 200 GeV/c. The minimum distance of a track to a primary vertex, the impact parameter, is measured with a resolution of  $(15 + 29/p_T) \mu\text{m}$ , where  $p_T$  is the component of the momentum transverse to the beam, in GeV/c.

37 Different types of charged hadrons are distinguished using information from two ring-  
 38 imaging Cherenkov detectors [2]. Photons, electrons and hadrons are identified by a  
 39 calorimeter system consisting of scintillating-pad and preshower detectors, an electro-  
 40 magnetic calorimeter and a hadronic calorimeter. Muons are identified by a system  
 41 composed of alternating layers of iron and multiwire proportional chambers.  
 42 The event selection is performed by a trigger, which consists of a hardware stage, based  
 43 on information from the calorimeter and muon systems, followed by a software stage,  
 44 which applies a full event reconstruction.  
 45 In Run II, the alignment and calibration of all subdetectors is performed online in  
 46 between different stages of the high level trigger (HLT) and the results are immediately  
 47 applied to the reconstruction.

## 48 **2.1 RICH optical systems**

49 Both RICH1 and RICH2 have two sets of mirrors: the primary spherical mirrors, and  
 50 the secondary (a.k.a. plane, flat), much flatter mirrors. Cherenkov photons emitted by  
 51 a charged track are reflected off a primary mirror onto a secondary mirror, and from  
 52 there out of the LHCb acceptance onto the plane of photon detectors, which coincides  
 53 with the focal plane of the given part of the optical systems. The RICH1/RICH2 op-  
 54 tical systems consists of 4/56 primary and 16/40 secondary mirrors. The layouts of the  
 55 RICH optical systems are shown in Figure 1 [4, 5], while the structures of the mirror  
 56 arrays and their numbering are shown in Figures 6 and 7 of Section 3.  
 57 The right-handed coordinate system of each mirror segment is defined by placing the  
 58 origin at the centre of curvature with the  $x$ -axis pointing towards the mirror, the  $y$ -  
 59 axis pointing upwards and the corresponding  $z$ -axis being horizontal. Finally, the pivot  
 60 point for the software rotations around the  $y$ - and  $z$ -axes is at the centre of each mirror.  
 61 In order to achieve the optimal performance of the LHCb RICH detector we aim to  
 62 minimize the uncertainty,  $\sigma$ , associated with the measurement of a single photon Cher-  
 63 enkov angle. This is limited by four main sources of uncertainty outlined in Table 1.  
 64 Adding them in quadrature gives the minimal total uncertainty, which can be obtained  
 by having an optimal alignment of all optical components of the RICH detectors.

Table 1: Sources of uncertainty,  $\sigma$ , of the measurement of a single photon Cherenkov angle for  
 the three LHCb RICH radiators.

	$\sigma$ [mrad]	
	RICH1	RICH2
	C <sub>4</sub> F <sub>10</sub>	CF <sub>4</sub>
Emission point	0.8	0.2
Chromatic dispersion	0.9	0.5
Pixel size	0.6	0.2
Tracking	0.4	0.4
Total	1.5	0.7

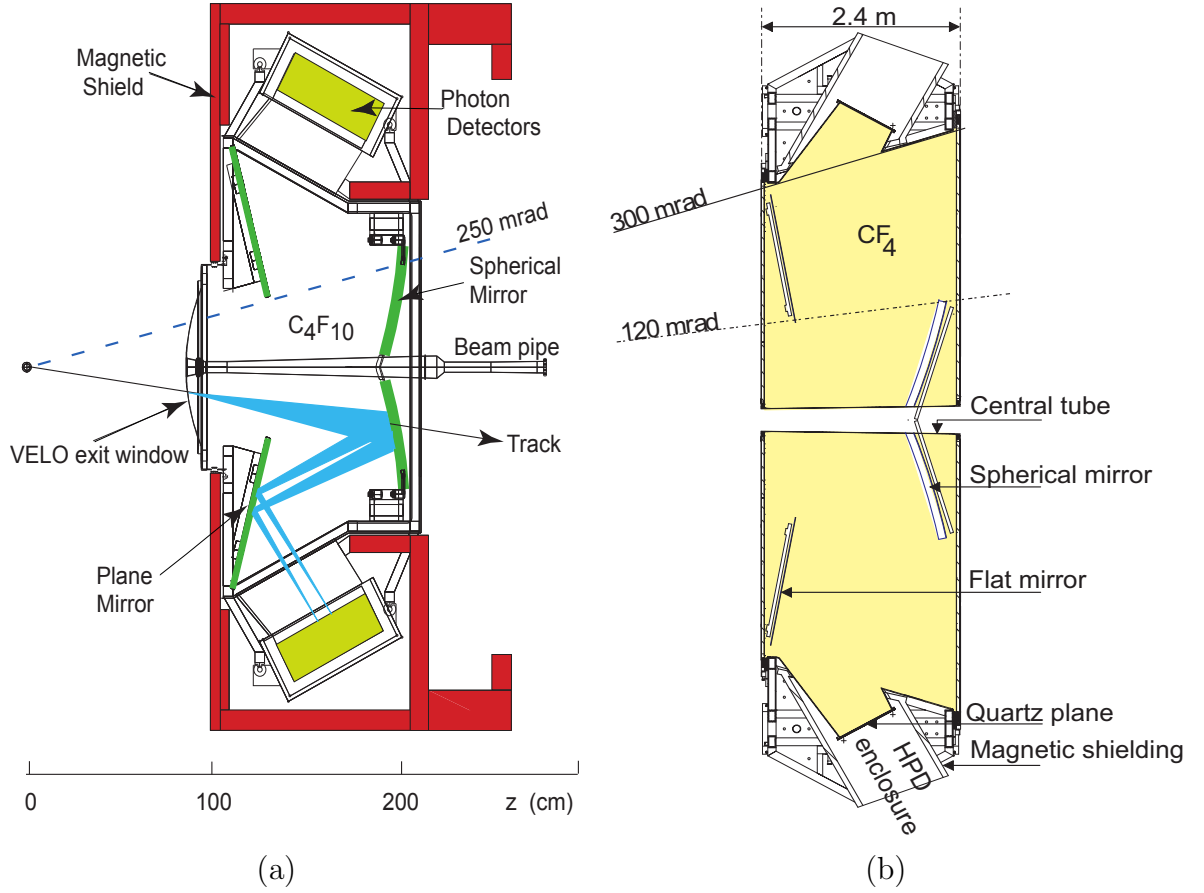


Figure 1: Schematic view of the LHCb RICH detectors and their optical systems: (a) side view of RICH1 and (b) top view of RICH2. Formation of a Cherenkov ring in the lower part of RICH1 is also drawn.

### 3 Method of alignment for the RICH optical system

An iterative, data-driven method for finding appropriate software compensations for the mirror misalignments was developed in the HERAb experiment [6]. The approach presented here builds on that method and is developed further to address the more complex design of the LHCb RICH system.

A misalignment in the LHCb RICH optical system manifests itself as a displacement of the observed Cherenkov ring against the expected one [7, 8] as can be seen in Figure 2. This can also be viewed as a discrepancy between the actual center of the Cherenkov ring - e.g. the center of the Cherenkov ring observed on the detector plane - and its expected position calculated from the projection of the track onto the detector plane using the orientation of the optical components given in the current LHCb conditions database.

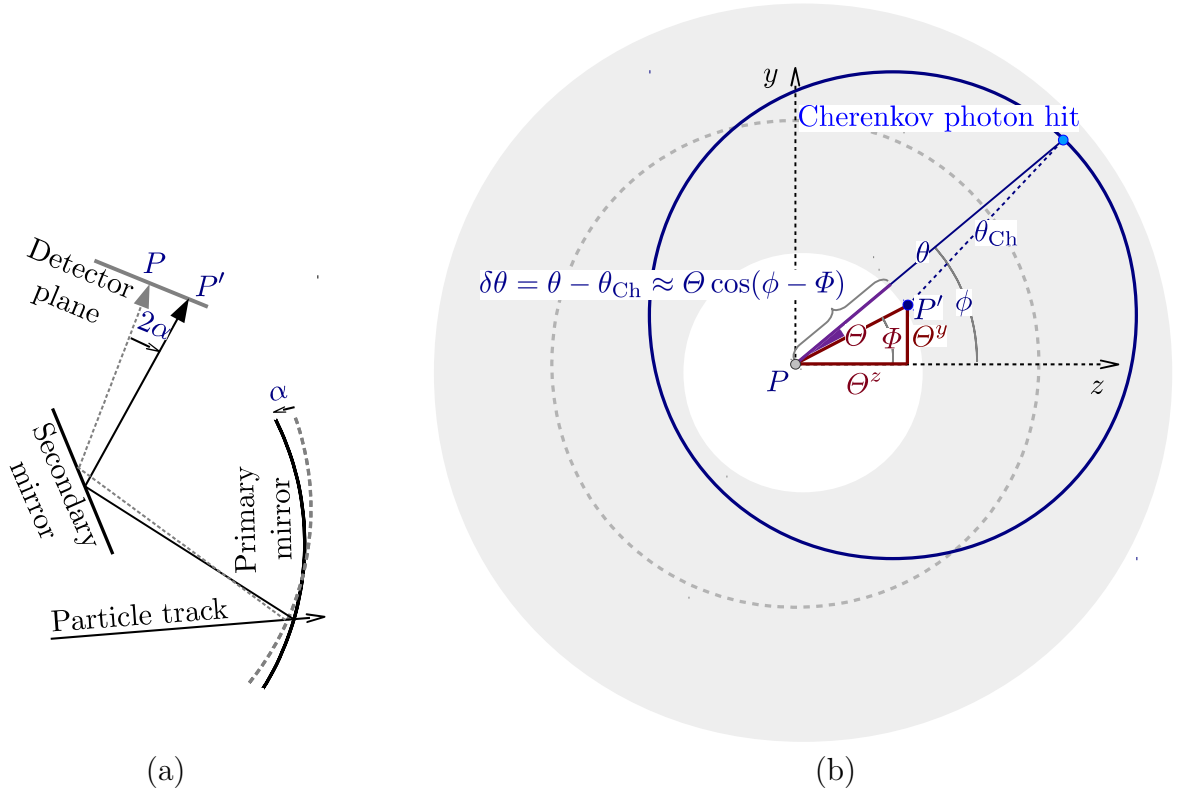


Figure 2: (a) Schematic drawing of how a rotational misalignment of a RICH mirror (primary mirror in this example) causes shift of the actual centre  $P'$  of the Cherenkov ring to  $P$  on the photon detector plane. The projection of the track is drawn for explanatory purpose and represents the position of the expected centre of the Cherenkov ring. (b) The expected Cherenkov angle  $\theta_{\text{Ch}}$  and the reconstructed Cherenkov angle  $\theta$  are displayed.  $P$  marks the position of the extrapolated track projection calculated without adjustments that would compensate any misalignments of the RICH mirrors, while  $P'$  is the actual position of the centre of the ring and displaced by  $\Theta^z$  and  $\Theta^y$  with respect to  $P'$ . Cherenkov angles  $\theta$  are evaluated relative to  $P$ , and therefore, vary with  $\phi$ . The gray stripe represents area around the expected ring from which the photon hits are reconstructed. The width of this stripe is empirically chosen wide enough to cover the actual shifted (and somewhat smeared) ring of hits from a given track. Inevitably, the “noise” background photon hits in this area are also “reconstructed”.

79 In order to observe and quantify the misalignment the quantity  $\delta\theta$

$$\delta\theta(\phi) = \theta(\phi) - \theta_{\text{Ch}}, \quad (2)$$

80 – where  $\theta(\phi)$  is the the measured Cherenkov angle and  $\theta_{\text{Ch}}$  the expected Cherenkov  
 81 angle – is plotted against the azimuthal angle  $\phi$  (see Figure 2). For perfectly aligned  
 82 mirrors  $\delta\theta$  is independent of  $\phi$  but in case of a misalignment the distribution is approx-  
 83 imately sinusoidal in  $\phi$

$$\begin{aligned} \delta\theta_{p,s}(\phi) &\equiv [\theta(\phi) - \theta_{\text{Ch}}]_{p,s} \approx [\Theta \cos(\phi - \Phi)]_{p,s} \\ &= [\Theta \cos \Phi \cos \phi + \Theta \sin \Phi \sin \phi]_{p,s} \\ &= \Theta_{p,s}^z \cos \phi + \Theta_{p,s}^y \sin \phi \end{aligned} \quad (3)$$

84 where the factors  $\Theta_{p,s}^y$  and  $\Theta_{p,s}^z$  represent the misalignments on the detector plane in  $y$   
 85 and  $z$  for a given mirror combination with primary mirror  $p$  and secondary mirror  $s$ .  
 86 The misalignment factors  $\Theta_{p,s}^y$  and  $\Theta_{p,s}^z$  relate to the individual misalignments of the  
 87 primary and secondary mirror via the *magnification factors*

$$\begin{aligned} A_{p,s}^y \alpha_p^y + B_{p,s}^y \beta_s^y + a_{p,s}^y \alpha_p^z + b_{p,s}^y \beta_s^z &= \Theta_{p,s}^y \\ A_{p,s}^z \alpha_p^z + B_{p,s}^z \beta_s^z + a_{p,s}^z \alpha_p^y + b_{p,s}^z \beta_s^y &= \Theta_{p,s}^z \end{aligned} \quad (4)$$

88 where  $\alpha_p^y$ ,  $\alpha_p^z$ ,  $\beta_s^y$  and  $\beta_s^z$  are the actual tilts of the primary and secondary mirrors  
 89 around the  $y$ - and  $z$ -axis with respect to a given database. The magnification factors  
 90  $A_{p,s}^y$ ,  $B_{p,s}^y$ ,  $a_{p,s}^y$  and  $b_{p,s}^y$  ( $A_{p,s}^z$ ,  $B_{p,s}^z$ ,  $a_{p,s}^z$  and  $b_{p,s}^z$  for the  $z$ -axis) translate the effect of a  
 91 tilt of the mirrors onto the detector plane (see Section 3.3).  
 92 After all individual mirror tilts have been calculated a new database with the mirror  
 93 orientations is created. It is useful to apply the alignment procedure iteratively to the  
 94 same data sample, each time with the new database produced by the previous align-  
 95 ment. The alignment procedure is considered to have converged after no mirror has  
 96 been found to have a misalignment greater than a chosen convergence criteria.  
 97 An overview of the entire alignment procedure can be seen in Figure 3 while different  
 98 details of the procedure are explained in the sections below.

### 99 3.1 Track and photon selection

100 The events that the tracks and their photons are taken from are preselected. More  
 101 information about the preselection and its implementation is given in Section 4.  
 102 In order to most accurately predict the Cherenkov angle for a given track some selec-  
 103 tion criteria are applied to the tracks themselves and to the photon candidates that  
 104 make it into the  $\delta\theta$  vs.  $\phi$  histograms.  
 105 High-momentum tracks are selected where the assumption can be made that the Cher-  
 106 enkov angle is saturated and therefore does not depend on the particle type any more.  
 107 Figure 4 and Equation 3 show the dependency of the Cherenkov angle of the mo-  
 108 mentum  $p$  for different types of particles with mass  $m$  in a radiator with refractive  
 109 index  $\eta$ .

$$\theta_{\text{Ch}} = \arccos \left( \frac{1}{\eta} \sqrt{\left(\frac{m}{p}\right)^2 + 1} \right) \quad (5)$$

110 In the case of high energy tracks all particles are assumed to have the the mass of a  
 111 pion and the expected Cherenkov angle is calculated under that hypothesis.  
 112 The photon hits chosen to fill the  $\delta\theta$  vs.  $\phi$  histograms are chosen from a ring-shaped  
 113 area around the expected center of the Cherenkov ring (see Figure 2). The ring's width  
 114 is chosen to be big enough to cover the area of a shifted Cherenkov ring from a poten-  
 115 tially misaligned mirror combination.  
 116 In the calculation of  $\delta\theta$  for the histograms the value for  $\theta(\phi)$  is needed. This value is  
 117 obtained by matching a photon hit on the detector plane to a track and calculating the

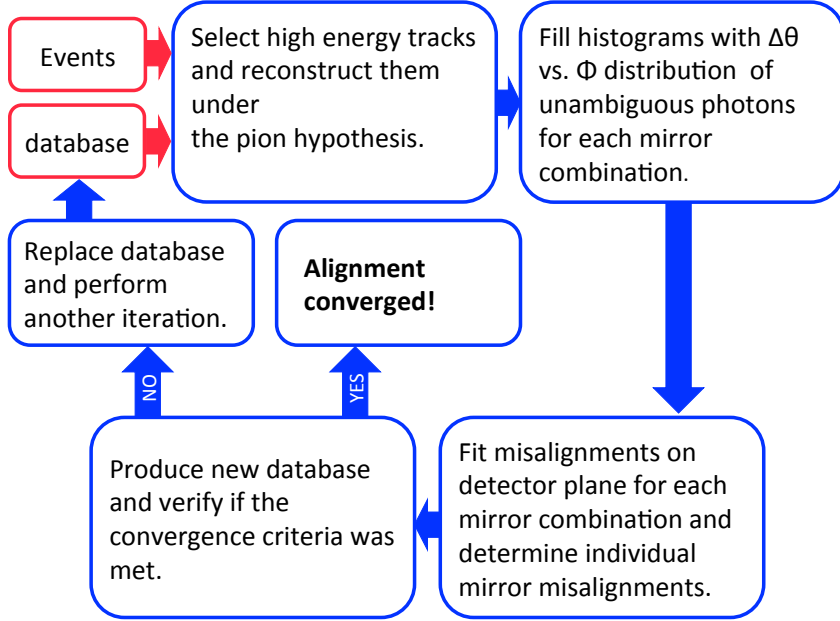


Figure 3: Overview of the entire alignment procedure. The alignment starts from a sample of events and usually from the mirror orientation given in the LHCb conditions database. From there high energy tracks are reconstructed under the pion hypothesis (see Section 3.1). Then the  $\delta\theta$  vs.  $\phi$  histograms are filled for each mirror combination selected for the alignment procedure (see Section 3.4) and fitted to get the misalignments on the detector plane. With these the individual mirror misalignments are determined and a new database containing the corrected mirror orientations is created. If the convergence criteria is reached the alignment procedure is finished, if the criteria has not been reached the newly made database is used for the reconstruction of the same events and the entire procedure is repeated.

Cherenkov angle. This requires an assumption about where along the track the Cherenkov photon was emitted. Since this is an intrinsically unknown quantity the assumption is made that the photon was emitted in the middle of the track. This introduces a source of noise from photons falsely associated with a given track. An analysis of MC events has shown [6] that it is possible to reduce this noise by only reconstructing *unambiguous* photon hits. A photon hit is *unambiguous* if it will be reflected by the same primary and secondary mirror independently of where along the particle track it was emitted. Therefore only unambiguous photon hits are chosen to be used in the alignment procedure in the  $\delta\theta$  vs.  $\phi$  histograms.

### 3.2 Method for fitting the $\delta\theta$ vs. $\phi$ distributions

For every chosen combination of primary mirror  $p$  and secondary mirror  $s$ ,  $\delta\theta$  is plotted against  $\phi$ . Each of these two-dimensional distributions is divided into 20 bins in  $\phi$ . Inside each  $\phi$  bin the  $\delta\theta$  distribution is fitted with a Gaussian plus a second order polynomial that represents the background photons. In accordance with Equation 3 the  $\phi$  dependence of the position of the Gaussian peak for a given mirror combination  $(p, s)$



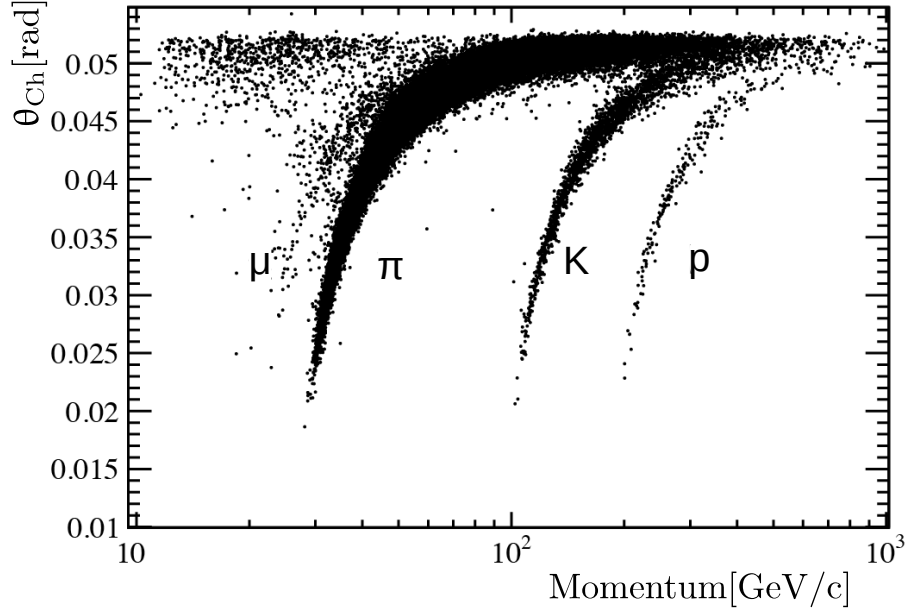


Figure 4: Cherenkov angle  $\theta_{\text{Ch}}$  against track momentum, for tracks traversing the RICH1 gaseous radiator. Muons, pions, kaons and protons are visible. As the track momentum increases, all particles tend towards the same  $\theta_{\text{Ch}}$ , known as the saturated Cherenkov angle.

133 is approximated by

$$\delta\theta_{p,s}(\phi) = \Theta_{p,s}^z \cos \phi + \Theta_{p,s}^y \sin \phi. \quad (6)$$

134 Equation 6 is used as a bond when fitting all the 20 slices jointly.

135 The fitting is done by means of the ROOT framework [9], in particular, using the  
 136 MINUIT minimization package. An example of a  $\delta\theta$  vs.  $\phi$  histogram for a specific mirror  
 137 combination in RICH1, including the fitted sinusoidal of Equation 6 is shown in Figure 5, before alignment and after the alignment.

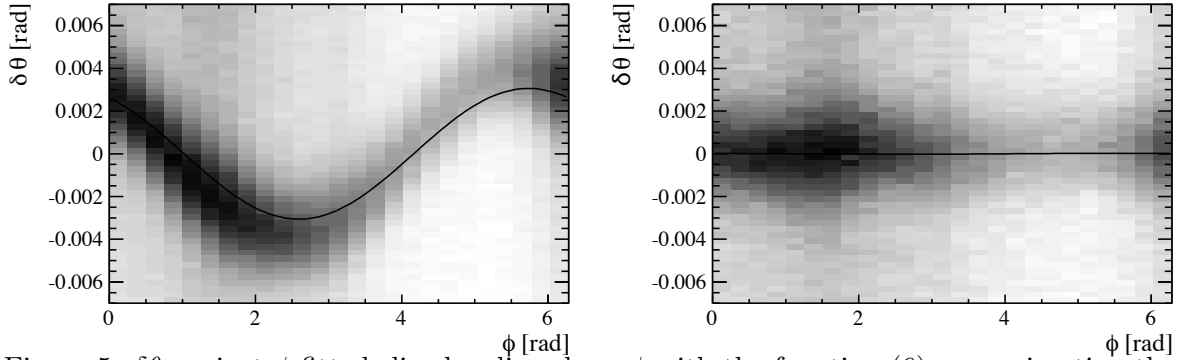


Figure 5:  $\delta\theta$  against  $\phi$  fitted slice-by-slice along  $\phi$  with the function (6) approximating the position of the Gaussian peaks on the  $\phi$ - $\delta\theta$  plane for the combination of primary mirror 0 and secondary mirror 1 of the RICH1. The originally misaligned mirror combination is represented on the left while the right plot shows the same mirror combination after the alignment procedure.

138

### 3.3 Magnification factors

The magnification factors relate the tilts of the individual mirrors to the misalignment that can be observed in the detector plane. The effect of the magnification factors can be demonstrated in a simplified manner by considering small rotations of primary and secondary mirrors around their  $y$ - axes. Those small rotations yield approximately the following displacement of the observable Cherenkov ring (as shown in Fig. 2):

$$l \Theta^y \approx l_{\text{pri}} 2 \alpha^y - l_{\text{sec}} 2 \beta^y, \quad (7)$$

where  $l$ ,  $l_{\text{pri}}$  and  $l_{\text{sec}}$  are lengths' of the paths of the photons to the photon detectors (from the emission point, from the primary mirror, and from the secondary mirror, respectively). Dividing this by the total photon path  $l$  yields

$$\Theta^y \approx \frac{2 l_{\text{pri}}}{l} \alpha^y - \frac{2 l_{\text{sec}}}{l} \beta^y \approx A^y \alpha^y + B^y \beta^y \quad (8)$$

where the factors in front of the actual mirror tilts  $\alpha^y$  and  $\beta^y$  are defined to be the magnification factors. The above equation is for illustrative purposes only and represents a simplified view because it doesn't take effects from rotations around the alternative (here  $z$ -) axis into account. The full expression used in the alignment procedure is shown in Equation 4.

The magnification factors are determined using a data-driven method. Eight independent calibrational rotations (positive/negative rotations about the  $y$ - /  $z$ - axis for the primary and secondary mirrors) are introduced. Then the resulting misalignment on the detector plane is measured and used to solve Equation 8 for the magnification factors. The final value of each magnification factor is arithmetical mean of the two corresponding values obtained with the calibrational rotations in opposite directions.

The size of each calibrational rotation for RICH1 is chosen to be  $\pm 0.7$  mrad in order to sufficiently determine the magnification factors. This choice is motivated by the fact that the Cherenkov angle resolution for RICH1 is around 1.6 mrad. Due to the smaller resolution of 0.7 mrad in RICH2, the size of its calibrational rotations is chosen to be  $\pm 0.3$  mrad.

### 3.4 Determining individual mirror misalignments

The fits to the  $\delta\theta$  vs.  $\phi$  distributions yield the misalignments in  $y$  and  $z$  on the detector plane for a given mirror combination. In order to determine the actual positioning of the mirrors for the LHCb conditions database, the misalignments of the individual primary and secondary mirrors are needed. This gives a system with more unknowns (individual mirror misalignments in  $y$  and  $z$ ) than equations. However, an optimal alignment can be achieved if each component of the optical system is properly aligned relative to all others. Therefore all mirrors only need to be aligned with respect to each other.

### 3.4.1 RICH1 alignment

The geometry of the LHCb RICH1 detector restricts the number of populated mirror combinations to 16, as shown in Figure 6. Photons reflected off a primary mirror are reflected off one of four secondary mirrors that form a group, unique to that primary mirror. Each of the four quadrants contain a single primary mirror and four secondary mirrors.

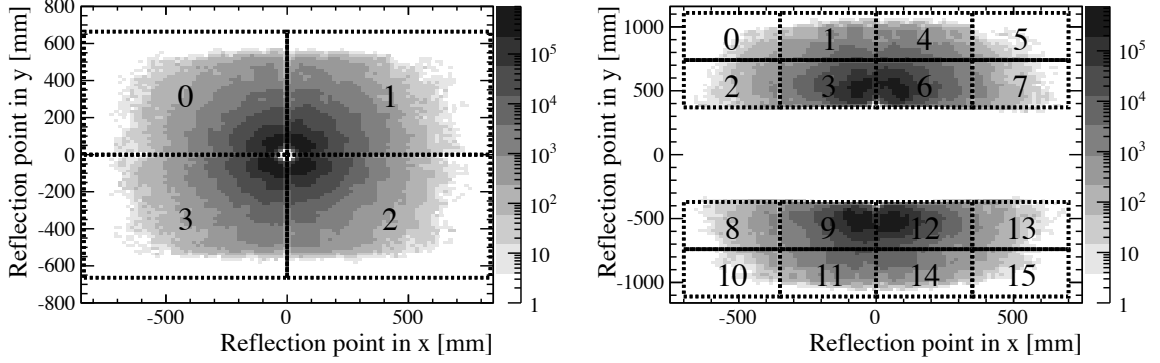


Figure 6: RICH1 mirror numbering scheme and reflection point distribution of photons off RICH1 primary mirrors (left) and secondary mirrors (right). The photon population across mirrors is not uniform with the higher populated mirrors laying closest to the beam-pipe.

Thus for each quadrant there are four equations and five unknowns for the  $y$ - and  $z$ -direction respectively. These are shown here for the example of the quadrant of primary number 0 in the  $y$ -direction

$$\begin{aligned} A_{0,0}^y \alpha_0^y + B_{0,0}^y \beta_0^y &= \Theta_{0,0}^y \\ \vdots & \quad \quad \quad \vdots \\ A_{0,3}^y \alpha_0^y + B_{0,3}^y \beta_3^y &= \Theta_{0,3}^y. \end{aligned}$$

Since the mirrors only need to be aligned with respect to each other the primary mirrors are excluded from the adjustment procedure, i.e. it is assumed that  $\alpha_0^y = 0$ . The misalignment of the secondary mirrors are directly calculated from  $\beta_s^y = \Theta_{0,s}^y / B_{0,s}^y$  and thus contain a compensation for the misalignment of their respective primary mirrors.

### 3.4.2 RICH2 alignment

The geometrical layout of the RICH2 detector is significantly different to that of RICH1 in that a given primary mirror can reflect photons onto several secondary mirrors and a given secondary mirror can receive photons from different primary mirrors. The mirrors can only be divided into two decoupled systems: 48 mirrors on the left side of the beam, and 48 mirrors on the right side of the beam as can be seen in Figure 7. This gives 96 unknown parameters for each side (tilts around  $y$ - and  $z$ - axes for each mirror) from which only 47 out of the 48 possible tilts are independent, since a simultaneous rotation of all primary mirrors by one angle and all secondary mirrors by the corresponding

angle in the opposite direction will not change the position of the Cherenkov ring on the detector plane.

Each mirror only reflects/receives photons onto/from a couple of adjacent mirrors of the opposite kind. Thus there are still many more unknowns than there are equations. As for RICH1 the fact is used that all mirrors only have to be adjusted with respect to each other. For RICH2 that means that for each side one mirror is chosen to stay fixed while all other mirrors are aligned with respect to it by a chain of equations linking all mirrors together. There are different possibilities of connecting all mirrors and the one chosen for the alignment procedure is the one that maximises the number of photons exchanged between mirrors. The way the mirrors are chosen to be linked for the left half of RICH2 can be seen in Figure 8. Additionally the involved mirror combinations are listed in Tables 2 and 3 grouped by primary and secondary mirrors respectively. The result is a system of 94 linear equations (47 combinations of Equations 4) which is solved algebraically using the substitution method between different mirror combinations and Cramers's rule within the two equations for one mirror combination.

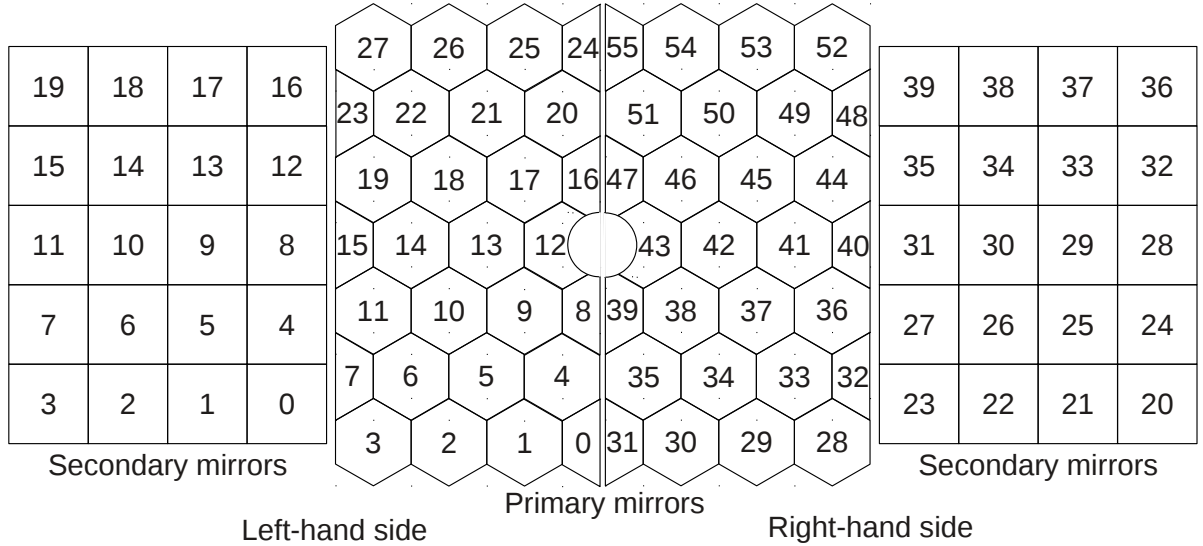


Figure 7: RICH2 mirror segmentation numbering scheme, viewed along the beam with the beampipe at the center.

## 4 The Online Alignment Framework

### 4.1 Dataflow in Run II

The LHCb trigger strategies for the Run I and Run II data taking periods are shown in Figure 9.

In Run I the online event reconstruction was simpler and faster than the reconstruction used offline and did not include any information about the particle identification (PID).

In order to have the same reconstruction online and offline as well as using the PID

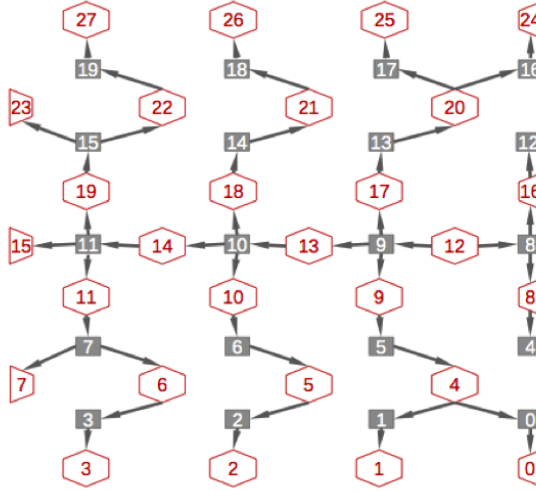


Figure 8: Illustration of how the primary and secondary mirrors of the left half of RICH2 are linked in order to align them with respect to each other starting by fixing primary mirror 12.

Table 2: The 47 chosen  $p, s$  (primary,secondary) mirror combinations grouped by primary mirror for the left-hand side of RICH2.

27,19	26,18	25,17	24,16
	22,19 22,18	21,17	20,16
23,15	22,14	21,13	20,12
19,15	18,14	17,13	16,12
19,11	18,10	17,9	16,8
15,11	14,11 14,10	13,10 13,9	12,9 12,8
11,11	10,10	9,9	8,8
11,7	10,6	9,5	8,4
7,7	6,6	5,5	4,4
	6,3 6,2	5,1	4,0
3,3	2,2	1,1	0,0

217 information in the HLT2 the data-taking strategy has been amended for Run II. As  
 218 in Run I a rate of 1 MHz of events passes the level-0 trigger (L0) and is passed on to  
 219 the first high level trigger stage (HLT1). There the events are partially reconstructed  
 220 and accepted events are written to disk. At this stage the different alignments are run  
 221 on a dedicated part of the buffered data. In case of a big shift in alignment constants  
 222 the new constants are propagated to the LHCb conditions database and used in the  
 223 subsequent processing of the events by the second high level trigger (HLT2).  
 224 The alignment tasks being performed on the data are - in the order they are being  
 225 run - VELO alignment, tracker alignment, RICH alignment and finally muon chamber  
 226 alignment. Each alignment has its own dedicated HLT1 line which collects a given  
 227 number of events at the beginning of each fill (see Section 4.2 for the RICH lines). It  
 228 has been found that  $\sim 1$  M events for RICH1 and  $\sim 2$  M events for RICH2 is sufficient  
 229 to produce stable results. Once enough events have been collected the alignment is

Table 3: The 47 chosen  $p, s$  (primary,secondary) mirror combinations grouped by secondary mirrors for the left-hand side of RICH2.

	27,19		26,18		25,17		24,16
	22,19		22,18		21,17		20,16
	23,15		22,14		21,13		20,12
	19,15		18,14		17,13		16,12
	19,11		18,10		17,9		16,8
15,11	14,11	14,10	13,10	13,9	12,9		12,8
	11,11		10,10		9,9		8,8
	11,7		10,6		9,5		8,4
	7,7		6,6		5,5		4,4
	6,3		6,2		5,1		4,0
	3,3		2,2		1,1		0,0

230 started.

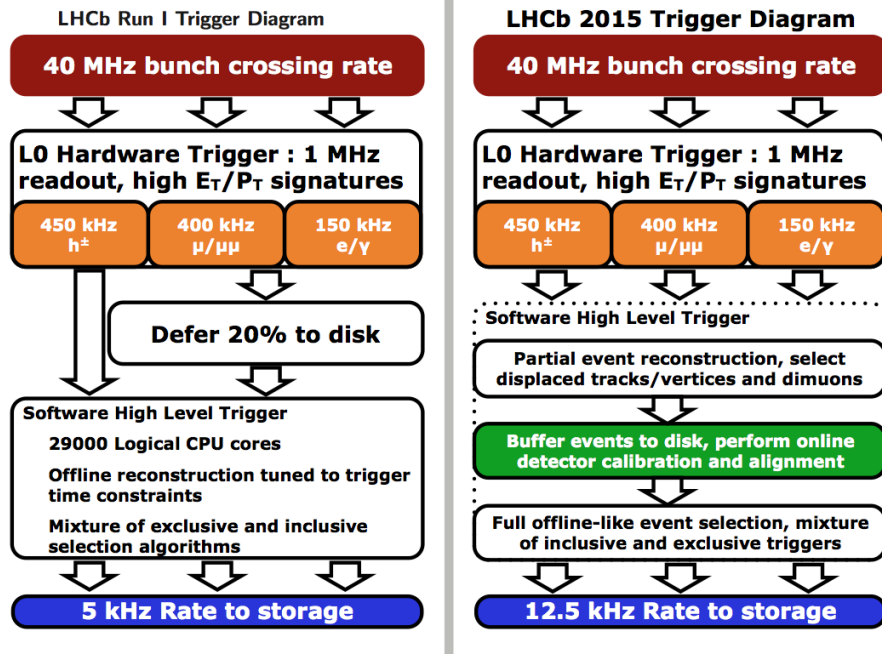


Figure 9: LHCb dataflow for Run I (left) and Run II (right). In Run II the data is buffered after HLT1 and an alignment is performed for each fill. The HLT2 will then process the buffered events with the updated alignment constants.

## 4.2 HLT1 selection for the RICH mirror alignment

In order to determine the misalignments on the detector plane and subsequently the individual mirror misalignments the  $\delta\theta$  vs.  $\phi$  histograms for each mirror combination have to contain enough entries for the fits described in Section 3.2 to converge. The

235 minimum condition for a successful fit has been found to be that 16 of the 20 bins in  $\phi$   
 236 have to contain at least 300 entries.  
 237 This is accomplished by having two dedicated HLT1 selections, one each for RICH1  
 238 and RICH2. The lines trigger on high energy particle tracks whose Cherenkov photons  
 239 would populate the mirror combinations containing the fewest photons. The other mir-  
 240 ror combinations are then populated by the rest of the tracks in the events.  
 241 The variables used in the selection are the track momentum  $p$ , the transverse track  
 242 momentum  $p_T$ , the pseudorapidity  $\eta$ , the goodness of fit for the track  $\chi^2$  and the polar  
 243 angle of the track  $\phi$ . The selection criteria of tracks that are triggered upon are listed  
 244 in Table 4.

Table 4: Trigger criteria for the HLT1 line for RICH1 and RICH2. Events that are accepted by these trigger lines need to have at least one track that satisfies the cuts listed below.

	RICH1	RICH2
momentum $p$	$p > 20 \text{ GeV}$	$p > 40 \text{ GeV}$
transverse momentum $p_T$	$p_T > 0.5 \text{ GeV}$	$p_T > 0.5 \text{ GeV}$
pseudorapidity $\eta$	$1.6 < \eta < 2.04$	$2.65 < \eta < 2.80$
track $\chi^2$	$\chi^2 < 2$	$\chi^2 < 2$
polar angle $\Phi$	$-2.65 < \Phi < -2.30$	$-2.59 < \Phi < -2.49$
	$-0.80 < \Phi < -0.50$	$-0.65 < \Phi < -0.55$
	$0.50 < \Phi < 0.80$	$0.55 < \Phi < 0.65$
	$2.30 < \Phi < 2.65$	$2.49 < \Phi < 2.59$

### 245 4.3 The Alignment Farm

246 All alignments are run on the alignment farm. The alignment farm consists of approx-  
 247 imately 1700 CPUs, called *analysers* and a central node called the *iterator*.  
 248 The data taken from the HLT1 selection for the RICH alignments is stored evenly dis-  
 249 tributed over the analysers until it can be processed by HLT2. The analysers perform  
 250 the event reconstruction with a database provided to them by the iterator and fill the  
 251  $\delta\theta$  vs.  $\phi$  histograms mentioned in Section 3. Apart from providing the database with  
 252 the desired mirror orientations the iterator also performs the fits on the histograms,  
 253 determines the individual mirror misalignments, produces a new database and decides  
 254 whether the alignment procedure has converged or whether another iteration has to be  
 255 performed. If the latter is the case, the iterator will make the new database available to  
 256 the analysers (for more details see Section 4.5).  
 257 The advantage of having a system consisting of about 1700 nodes distributed over 50  
 258 farms is that the event reconstruction can happen in parallel and is therefore very fast.  
 259 This parallel processing is asynchronous and has to be coordinated between the indi-  
 260 vidual analysers and the iterator which is described in the next section.

## 4.4 The Control Flow

The execution of the alignment tasks is under the control of the LHCb Experiment Control System (ECS), and is implemented as a *finite state machine*, which is illustrated in Figure 10. The principle of a finite state machine means that each component of the system (here every individual analyser and the iterator) has to be in one of a finite number of states at all times. The states used for the alignment procedure are also shown in Figure 10, such as “READY”, “RUNNING” and “PAUSED”. The alignment is then steered by the *run control* that can see all the components and their individual states and can send commands. Those commands will be received by the individual components and they will act accordingly. For a given state only a certain number of commands are possible - for example if the component is in state “PAUSED” it can only receive the commands “continue” and “stop”. If a command is received the component will go from its state into the state declared by Figure 10. When in a new state the component will usually perform a task and then set itself into another state once finished so that the run control is aware of this task being completed.

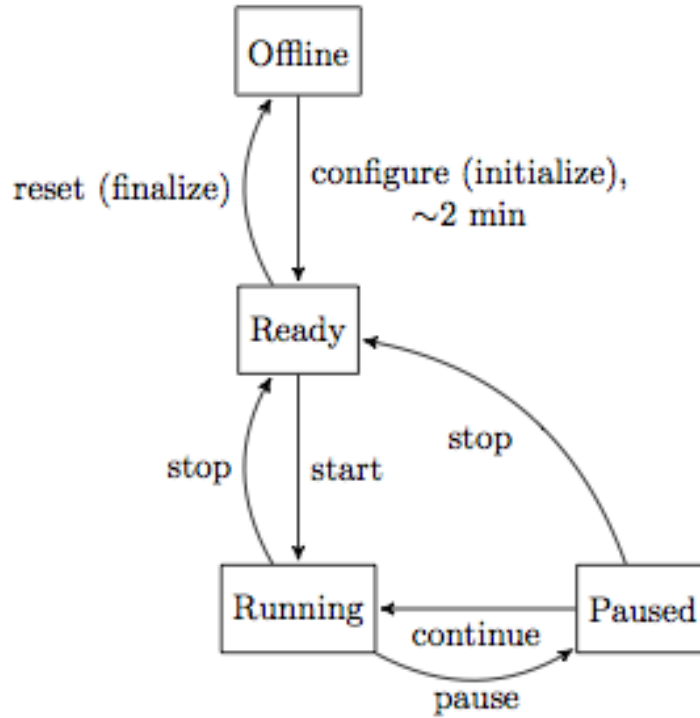


Figure 10: Example of one component within a system functioning under the principle of a finite state machine. The boxes show the states the component is in while the arrows show the commands the component gets from the run control.



## 4.5 Implementation of the RICH Mirror Alignment for Run II

The interplay between the iterator, one example analyser and the run control during the course of the alignment of a RICH detector is shown in Figure 11.

The individual analysers and the iterator all follow the same sequence of states, namely the one shown in Figure 10. When the alignment is being started the run control sends the command to “configure” to both the iterator and all analysers. All components will go into state “CONFIGURING” while setting up to run the alignment. For the analysers this means that they read in the configuration for the reconstruction of the events, while the iterator sets up a directory in which all files for this alignment are saved.

Each component goes into state “READY” when it is done configuring. When all tasks are in the “READY” state, the iterator makes an initial set of alignment constants available to the analysers and then updates its state to “RUNNING”. The analyzers are then sent the “start” command, update their state to “RUNNING” and start reconstructing the data stored on them. Each analyser that has completed processing its data updates its state to “PAUSED”, and once they have all reached this state, the run control sends the stop command and they update their states to “READY”. The iterator is then sent the “pause” command, collects and combines the histograms produced by the analyser tasks and performs the fits. It then calculates the individual mirror misalignments and produces a new database containing the mirror orientations. The it either indicates that conversion has been reached by updating its state to “READY”, or that further iteration is required by updating its state “RUNNING”. In the latter case the iterator will provide the new database to the analysers before changing its state and another iteration is started.

## References

- [1] LHCb collaboration, A. A. Alves Jr. *et al.*, *The LHCb detector at the LHC*, JINST **3** (2008) S08005.
- [2] M. Adinolfi *et al.*, *Performance of the LHCb RICH detector at the LHC*, Eur. Phys. J. **C73** (2013) 2431, [arXiv:1211.6759](#).
- [3] LHCb collaboration, R. Aaij *et al.*, *LHCb detector performance*, Int. J. Mod. Phys. **A30** (2015) 1530022, [arXiv:1412.6352](#).
- [4] LHCb Collaboration, *LHCb RICH technical design report*, CERN-LHCC-2000-037.
- [5] LHCb Collaboration, *LHCb technical design report: reoptimized detector design and performance*, CERN-LHCC-2003-030.
- [6] A. Gorisek, P. Krizan, S. Korpar, and M. Staric, *Alignment of the HERA-B RICH optical system with data*, Nucl. Instrum. Meth. **A433** (1999) 408.

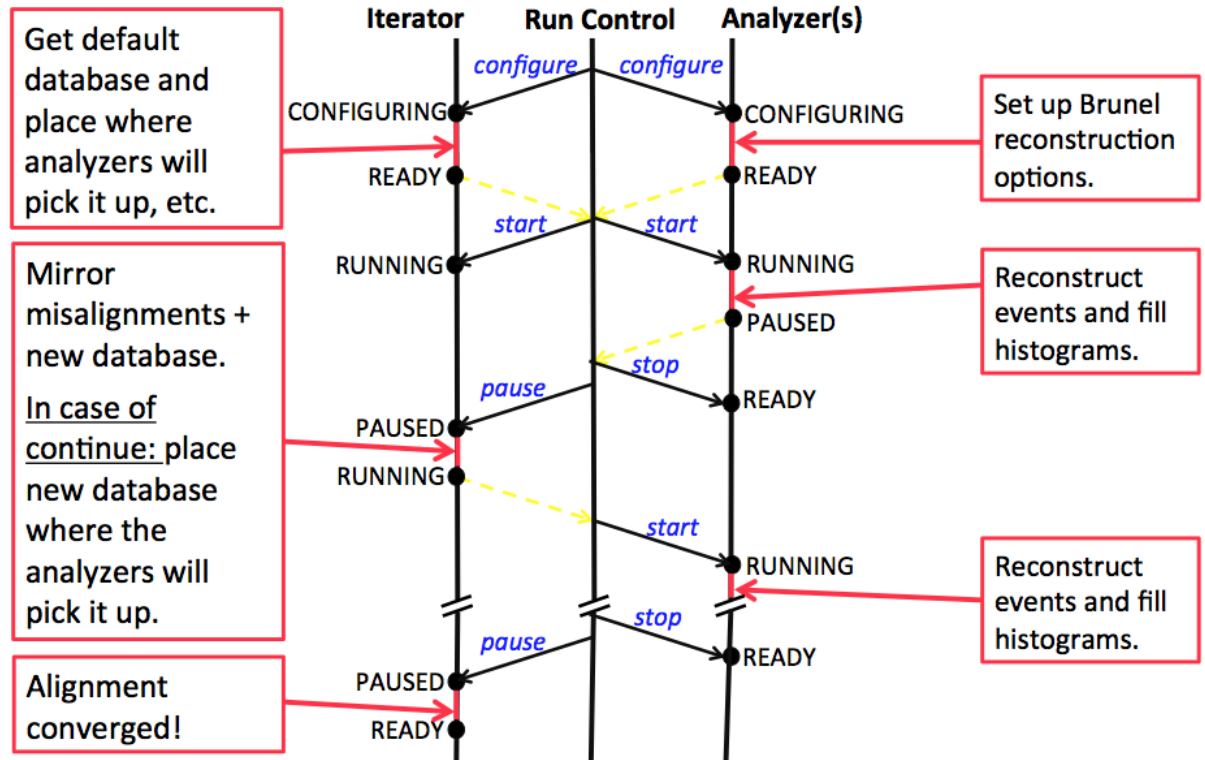


Figure 11: Interplay between the iterator, one example analyser and the run control during the RICH alignment procedure. The analysers reconstruct the data and produce the histograms that the iterator evaluates. The run control makes sends commands to the iterator and the analysers to make sure the alignment procedure happens in the necessary sequence.

- 312 [7] A. Papanestis, *The calibration and alignment of the LHCb RICH system*, Nucl. Instrum. Meth. **A595** (2008) 248.
- 313
- 314 [8] W. Baldini *et al.*, *LHCb alignment strategy*, LHCb-2006-035.
- 315 [9] I. Antcheva *et al.*, *ROOT: A C++ framework for petabyte data storage, statistical analysis and visualization*, Comput. Phys. Commun. **182** (2011) 1384.
- 316